scientific reports

Check for updates

OPEN

Identifying RAGE inhibitors as potential therapeutics for Alzheimer's disease via integrated in-silico approaches

Inderjeet Bhogal, Vaishali Pankaj & Sudeep Roy✉

Alzheimer's disease is a neurodegenerative disorder characterized by two hallmarks: amyloid beta plaques and neurofibrillary tangles. The receptor for advanced glycation end products (RAGE) is a multi-ligand receptor involved in the pathophysiology of various diseases including cancer, diabetes, cardiovascular diseases, and Alzheimer's disease (AD). Therefore, targeting RAGE could be an effective strategy to block RAGE signaling pathways. The present study aims to identify potential RAGE inhibitors against AD through comprehensive in-silico approaches. A total of 708,580 compounds were screened from numerous databases using structure-based virtual screening and ADMET evaluation. Further, the molecules with good glide scores were assessed by molecular docking studies. Subsequently, the top six ligands were subjected to molecular dynamic (MD) simulations for 100 ns and binding free energy calculations to check their stability with RAGE (PDB: 6XQ3). The per-residue decomposition analysis revealed that specific residues namely, GLY_20, ALA_21, LYS_39, GLU_50, LYS_52, ARG_98, GLN_100, LYS_110, ASN_112, and ARG_198 played a key role in the binding process. Furthermore, the trajectory analysis (DCCM and PCA) analyzed the dominant motions of residues and predicted the stability of protein-ligand complexes. In conclusion, the Hit-6 compound could be a promising candidate for targeting RAGE and deserves further consideration as an anti-Alzheimer drug.

Keywords Alzheimer's disease, Molecular dynamics, Virtual screening, MM-GBSA, RAGE inhibitors

Alzheimer's disease (AD) is a chronic degenerative disorder resulting from the progressive damage and dysfunction of the central nervous system including neurons. AD is the most common kind of dementia and may account for 60–70% of the 55 million dementia cases and this is anticipated to grow to 150 million by 2050[1]. The pathophysiology of AD can be characterized by the extensive presence of a large number of neuroinflammatory plaques composed of amyloid-beta (Aβ), and neurofibrillary tangles (NFT) of accumulated hyperphosphorylated tau (τ) protein[2]. The FDA-approved therapies for AD are classified as amyloid-targeting approaches and drugs that treat symptoms. The anti-amyloid drugs address the underlying problem instead of just focusing on the symptoms. Presently, there are two anti-amyloid antibody intravenous (IV) infusion therapies approved by FDA i.e., Donanemab[3] and Lecanemab[4] approved in July 2024 and January 2023 respectively that demonstrate the removal of Aβ from the brain of people living with early Alzheimer's. A third anti-amyloid therapy, Aducanumab[5] received accelerated approval in 2021 from the FDA to treat people with early Alzheimer's, but it was discontinued by its manufacturer, Biogen to focus on other drugs in 2024. On the other hand, there are only five FDA-approved drugs that treat AD symptoms and can be categorized as cholinesterase inhibitors (Donepezil, Rivastigmine, and Galantamine), glutamate regulators (Memantine), and Orexin receptor antagonists (Suvorexant). Cholinesterase inhibitors can block the enzyme acetylcholinesterase and are prescribed to patients with mild to moderate AD, while memantine is approved for patients with moderate to severe AD and it works by regulating the activity of glutamate. However, suvorexant is prescribed to treat insomnia and has shown to be effective in patients with mild to moderate AD[6]. Although the current medications cannot cure AD, they can only provide symptomatic relief and improve the quality of life of AD patients[7]. These circumstances have motivated scientists globally to pursue the development of novel potential drug candidates for treating AD.

The Receptor for Advanced Glycation End-products (RAGE) is a transmembrane receptor of the immunoglobulin superfamily with a molecular weight of 45–55 kDa, typically found in very low concentrations

Department of Biomedical Engineering, Faculty of Electrical Engineering and Communication, Brno University of Technology, Brno 616 00, Czech Republic. ✉email: roy@vut.cz

in healthy human tissues, including liver, kidney, lungs, nervous system, cardiovascular system, and immune system[8]. During inflammations or when there are increased levels of RAGE ligands like AGEs, S100/calgranulins, HMGB1 (high mobility group box-1 protein), amyloid-β (Aβ), and β-sheet fibrils, etc., RAGE expression is markedly elevated across various cellular systems[9]. The interaction of these ligands with RAGE stimulates several signaling pathways such as the diaphanous-related formin 1 (DIAPH1), mitogen-activated protein kinase (MAPK), phosphatidylinositol 3-kinase (PI3K)/AKT, and Toll-interleukin 1 receptor domain-containing adaptor protein (TIRAP). This results in RAGE-dependent NF-κB activation leading to the pathogenesis of various diseases[10]. A full-length human RAGE can be sub-divided into three domains: an extracellular domain (23–342 residues), a hydrophobic transmembrane domain (343–363 residues), and an intracellular domain (364–404 residues)[11]. The extracellular domain consists of three immunoglobulin domains, including the Variable domain (V-domain) consisting of 23–116 amino acid residues followed by two constant domains C1 (124–221 residues) and C2 (227–317 residues). It is evident from various studies that most of the RAGE ligands bind to the V and C1 domains including, S100/calgranulins, AGEs, Aβ and HMGB1, etc.

Recent studies have shown that inhibition of RAGE appears to be a promising approach to control RAGE-mediated signaling in multiple diseases including cancer, diabetes, kidney failure, cardiovascular disease, and neurodegenerative disorders[12]. A promising example of RAGE ligands, Azeliragon (TTP488) or PF-04494700[13] is an orally bioavailable small molecule that is currently under investigation, shown to block RAGE interactions with extracellular ligands such as S100B, HMGB1, and AGEs, thereby blocking the activation of the inflammatory signals. In addition, TTP488[14] has been shown to inhibit neurocognitive decline and reduce Aβ accumulation. FPS-ZM1[15,16] is another RAGE inhibitor that can inhibit the production of Aβ40 and Aβ42. Subsequently, it also suppresses β-secretase activity, which forms Aβ peptides, resulting in the reduction of brain damage[17]. In order to design new RAGE inhibitors that specifically target its VC1-domain, Kozlyuk et al. recently used a fragment-based approach to screen approximately 14,000 small fragments using nuclear magnetic resonance (NMR) spectra. They discovered three top binders (V6Y, V6M, and V6P) that can bind to three different sites on the RAGE receptor. With certain interactions stabilizing its binding conformation, the co-crystallized ligand V6Y from the PDB structure 6XQ3 functions as a known binder to the VC1 Domain of RAGE[18].

Therefore, blocking AGE-RAGE interactions may prevent an array of conditions such as neuroinflammation, synaptic and neuronal dysfunction, and cognitive impairment caused by AGE accumulation and RAGE-dependent signaling.

In the present study, we used structure-based virtual screening to identify structurally diverse therapeutic compounds capable of effectively blocking the interactions between RAGE and other proteins or ligands for the treatment of Alzheimer's disease. We performed the virtual screening to filter the compounds from several databases and the top-scoring hits were further employed for molecular docking studies. The top six screened compounds were considered for molecular dynamics simulations, and binding free energy calculations using the MM-GBSA method to identify the potential hit compounds that could inhibit the RAGE interactions with its ligands. Moreover, the physicochemical parameters and druglike ness of the top six screened compounds were also carried out by utilizing ADMET studies.

Materials and methods

All the molecular modeling studies were performed using the commercial Schrodinger Drug Discovery Suite (Release 2024-1). It encompasses "Virtual Screening" using the Glide tool, "Induced Fit Docking" and "MM-GBSA free energy calculations" using the PRIME module, and "Molecular Dynamics" using the Desmond tool. The ADMET profiling was done using the freely available web server ADMETLab 2.0.

Protein selection and preparation

The X-ray crystallographic structure of the target protein the Receptor for Advanced Glycation End Products (RAGE) VC1 domain (PDB Id: 6XQ3; Resolution 1.71 Å) in complexed with V6Y was obtained from the Protein Data Bank (PDB) (https://www.rcsb.org/)[19] and used as a target for virtual screening. The protein structure was prepared using the interactive mode of the "Protein Preparation Workflow" module[20] of the Schrodinger suite. The protocol included adding missing hydrogen atoms, assigning bond orders, optimizing hydrogen bonds, deleting waters and heteroatoms, and minimizing restrained energy using the Optimized Potentials for Liquid Simulations (OPLS4) force field. The prepared protein structure was further employed for the grid generation around the co-crystallized ligand by utilizing the "Receptor Grid Generation" panel of the Glide module[21] of the Schrodinger suite.

Dataset and library preparation

Ready-to-dock chemical compounds in 3D formats from various databases such as Enamine Fragment Libraries (27,600 fragments), Enamine Targeted Libraries (54,531 compounds), Enamine Bioactive Libraries (1040 compounds), Therapeutic Target Database (38,760 compounds), Selleckchem FDA-approved drug library (3105 compounds), Interbioscreen (Natural and Synthetic compounds) (555,013 compounds), ChemDiv (CNS BBB and Drug repurposing library) (27,331 compounds), and SwissSimilarity (ZINC drug-like, ZINC lead-like, and ZINC fragment-like) (1200 compounds) consisting of a total of 708,580 were downloaded in the SDF format accessed on 13 September 2023. The LigPrep[22] application of Schrodinger's Maestro was used to prepare the ligands by energy minimization and 3D structural optimization of the molecules using the OPLS4 force field. Further, Epik Classic was implemented to assign their ionization state at pH 7 ± 2 and generate tautomers of each compound.

Structure-based virtual screening

Virtual screening is a computational approach to identify potential drug candidates by screening various databases and it is a benchmark step in drug discovery. Virtual screening was accomplished by utilizing the Glide program of the Schrodinger suite. Protein-ligand flexible docking of the prepared libraries was done using the Virtual Screening Workflow (VSW) method of Glide. The compounds were pre-filtered based on QikProp properties and Lipinski's rule of five. Molecular docking was performed using standard precision (SP) and the more robust extra precision (XP) methods with default parameters. The docked complexes were post-processed and rescored based on the binding energy using the Prime/MM-GBSA tool[23] of the Schrodinger package. A total of 7086 XP hits were obtained from the virtual screening and the best hits from each library i.e., 30 top-scored hits based on glide gscore were further considered for molecular docking studies.

Molecular docking

Molecular docking studies were performed to investigate the binding pattern of the top thirty compounds against the VC1 domain of RAGE (PDB Id: 6XQ3) retrieved from the PDB. The crystal structure of the RAGE VC1 domain was prepared by utilizing the Protein Preparation Workflow of Schrodinger's Maestro. The interactive mode of the protein preparation workflow consists of four steps: pre-processing, diagnosis and analysis, optimizing H-bond assignments, minimization and water removal[24,25].

The docking protocol was validated by re-docking the co-crystallized ligand of the receptor into its original active site. Accordingly, a grid box was generated using the Receptor Grid Generation panel of the Glide module by selecting the centroid of the workspace ligand located at the binding site of the RAGE protein (6XQ3). A few constraints were applied to attain a reliable pose of ligands, including hydrogen bonds with LYS_39, LYS_52, ARG_98, and ASN_112 along with salt bridges and pi-cat interactions. The study revealed that docked poses of native inhibitors were superimposed with the co-crystallized ligand[26]. This indicates that the docking process is appropriate for the virtually screened compounds in the manner shown in Supplementary Fig. S1.

Eventually, the selected top six compounds were docked in the flexible RAGE protein using the Extra precision (XP) method within the generated grid via the Induced Fit Docking (IFD) panel of the Prime module. During IFD, a maximum of 20 poses were selected for each ligand and the side chains were trimmed automatically and the generated poses were minimized through backbone refinement within a distance of 4 Å. Finally, the docking scores and binding interactions of each pose of the virtually screened compounds were compared to the docked scores of the co-crystallized ligand, moreover, the important amino acid residue interactions were also analyzed and further employed for the molecular dynamic studies. Additionally, the Schrodinger suite's "Shape Screening" module[27] was used to determine the structural similarity between the native ligand and the top six hits found, as shown in Supplementary Fig. S2.

Molecular dynamic (MD) simulations

To determine the stability of the top six receptor-ligand complexes over time; an all atom molecular dynamics simulations were performed using the Desmond tool of Maestro included in the Schrodinger suite[28]. MD simulation is a three-step process that includes system builder, minimization, and molecular dynamics. In the system building step, an orthorhombic box with the dimensions of $10 \times 10 \times 10$ Å was defined around the receptor-ligand complexes, and the system was solvated with the simple point charge (SPC) water model. Secondly, to neutralize the system, 0.15 M concentrations of counter ions i.e., Na^+ and Cl^- were added. During minimization, the solvated system was minimized for 100 ps time to relax the complex to its minimum energy. Lastly, MD simulations were performed for 100 ns for the minimized and equilibrated systems under the NPT ensemble class i.e., normal pressure and temperature. The OPLS4 force field was used to perform the simulation by setting the temperature at 300 k and pressure at 1.01325 bar. Further, the Nose-Hoover chain thermostat approach was used to control the temperature, and the Martina-Tobias-Klien barostat technique was used to regulate the pressure.

Root mean square deviation (RMSD), root mean square fluctuation (RMSF), and protein-ligand contacts histogram plots were analyzed to determine the stability of the protein-ligand complexes in MD simulation. In addition, the dynamic cross-correlation matrix (DCCM), and principal component analysis (PCA) were performed to assess the MD trajectories at the residue level.

MM-GBSA free energy calculations

The receptor-ligand complexes' relative binding free energy was calculated using the Prime MM-GBSA (Molecular Mechanics/Generalized Born Surface Area) method of the Schrodinger suite (Release 2024-1). A highly negative MM-GBSA score indicates a strong correlation with experimentally determined data. The binding energy was estimated using the *thermal_mmgbsa.py* script provided by Schrodinger which splits the Desmond trajectory file into individual snapshots and calculates the average binding energy of each frame[29]. The binding free energy in MM-GBSA was calculated using the following equation:

$$\Delta G_{bind} = E_{complex(minimized)} - \{(E_{protein(minimized)} + G_{ligand(minimized)}\}$$

Residue decomposition analysis

The residue-wise binding energy contribution is a remarkable step in designing a new drug and defining pharmacophore features. The energy contributions of individual amino acids were examined to identify key amino acid residues involved in the ligand binding[30]. The residue-wise free energy calculations were performed through the *breakdown_MMGBSA_by_residue.py* script, which uses the MM-GBSA output and calculates each residue's average free energy contribution.

ADMET prediction

Assessing the ADME parameters is a crucial step in the drug discovery process before conducting experimental studies. While developing a molecule into an effective drug, the ADME parameters and toxicity prediction are key factors to be considered. The evaluation of ADMET (A: Absorption, D: Distribution, M: Metabolism, E: Excretion, and T: Toxicity) properties of the selected compounds was conducted by utilizing the ADMETlab 2.0 web server (https://admetmesh.scbdd.com/)[31]. The druggability of the compounds was predicated on various categories including physicochemical properties, medicinal properties, absorption, distribution, metabolism, excretion, and toxicity.

Results

Structure-based virtual screening

The X-ray co-crystallized structure of the RAGE VC1 domain with V6Y (PDB Id: 6XQ3) was obtained from the PDB database and selected as a model to perform molecular docking. A total of 708,580 3D compounds were downloaded in SDF format from numerous databases such as Enamine fragment libraries (Essential fragment library; High fidelity fragment library; DSI-poised library; MiniFrag library; Covalent fragment library; Fluorinated fragment library; Fully functionalized probe library; Natural product-like fragments; 3D shape diverse fragment library; PPI fragment library; Single pharmacophore fragments; Carboxylic acid fragment library; and Electrophilic covalent probe library), Enamine targeted libraries (CNS library; and BACE library), Enamine bioactive libraries (FDA approved drugs), Therapeutic target database (TTD) (all drugs), Selleckchem (FDA approved drug library), Interbioscreen screening compounds (Natural compounds; and synthetic compounds) and ChemDiv (CNS BBB library; Drug repurposing library). In addition, we also obtained similar structures to the native inhibitor (V6Y) from the SwissSimilarity (ZINC drug-like; ZINC lead-like; and ZINC fragment-like).

All the compounds were pre-filtered based on 51 QikProp properties followed by Lipinski's rule of five, and the ligands with reactive functional groups were also removed. Further, the compounds were considered for SP docking into the previously generated receptor grid of RAGE by utilizing the VSW panel of the Glide module. The crucial residues involved in binding RAGE with other inhibitors are preserved to LYS_52, ARG_98, and LYS_110 and included in the active site. To obtain more accurate results, and to reduce the chances of false positives, the SP docking hits were further subjected to the XP mode of docking and binding free energy calculations with Prime MM-GBSA and generated 3 poses per compound. A total of 7114 XP hits were acquired from the virtual screening and the hits with lower docking scores from each library were chosen for molecular docking studies. The detailed virtual screening results, indicating various chemical libraries and their size, and obtained virtual hits using the Extra Precision (XP) method are shown in Supplementary Table S1.

Molecular docking studies of the screened compounds

To identify potential inhibitors of RAGE, molecular docking studies were performed for the top thirty active hits obtained from the virtual screening protocol and five FDA-approved drugs for AD namely, Donepezil, Rivastigmine, Galantamine, Memantine, and Suvorexant. The molecules were suitably docked into the active site of RAGE and interacted with the selected amino acid residues via hydrogen bonds and hydrophobic interactions. The results were analyzed based on docking scores and showed that six compounds exhibited better binding affinity as compared to other hit compounds. The detailed XP docking results of the top six compounds (Hit-1 to Hit-6) and FDA-approved drugs compared to the native inhibitor (V6Y) including docking scores and interacting residues were shown in Table 1 and Supplementary Table S2 respectively. The 3D ligand interaction diagrams of the native ligand (V6Y) and the top six hit compounds with RAGE (PDB ID: 6XQ3) were illustrated in Fig. 1.

The docking protocol was validated by removing the co-crystallized ligand (V6Y) from the complex and re-docking it into the binding site of the RAGE VC1 domain (PDB Id: 6XQ3). A comparative study was performed to validate the docking analysis, the native ligand and the top-six compounds from the virtual screening were

S. no.	Ligand	IFD Score (kcal/mol)	Docking score (kcal/mol)	Glide energy (kcal/mol)	Glide e-model (kcal/mol)	H-bonds	Other interacting residues
1.	Native ligand (V6Y)	− 429.94	− 7.033	− 57.527	− 85.748	LYS_39, LYS_52, ARG_98, ASN_112	Salt bridges: LYS_39, LYS_52 Pi-Cat: LYS_110
2.	Hit-1	− 421.3	− 8.109	− 40.143	− 62.403	LYS_52, ARG_98, GLN_100, LYS_110, ASN_112	Salt bridges: LYS_52, LYS_110
3.	Hit-2	− 419.7	− 7.074	− 42.828	− 60.727	GLU_50, LYS_52, CYS_99	Salt bridges: GLU_50, LYS_52
4.	Hit-3	− 418.24	− 6.621	− 31.783	− 39.728	GLU_50	Salt bridges: GLU_50, LYS_52
5.	Hit-4	− 414.63	− 5.116	− 44.28	− 56.109	GLN_100, GLU_108	Pi-Cat: ARG_98
6.	Hit-5	− 424.84	− 10.008	− 55.576	− 68.315	GLN_24, LYS_52, ARG_98, ASN_112	Salt bridges: LYS_52, LYS_110 Pi-Cat: LYS_110
7.	Hit-6	− 427.9	− 9.109	− 52.893	− 59.885	MET_22, LYS_52, ARG_98	Salt bridges: LYS_52, ARG_98, LYS_110

Table 1. Molecular docking results of the native ligand (V6Y) and the top six hits against RAGE (PDB id: 6XQ3).

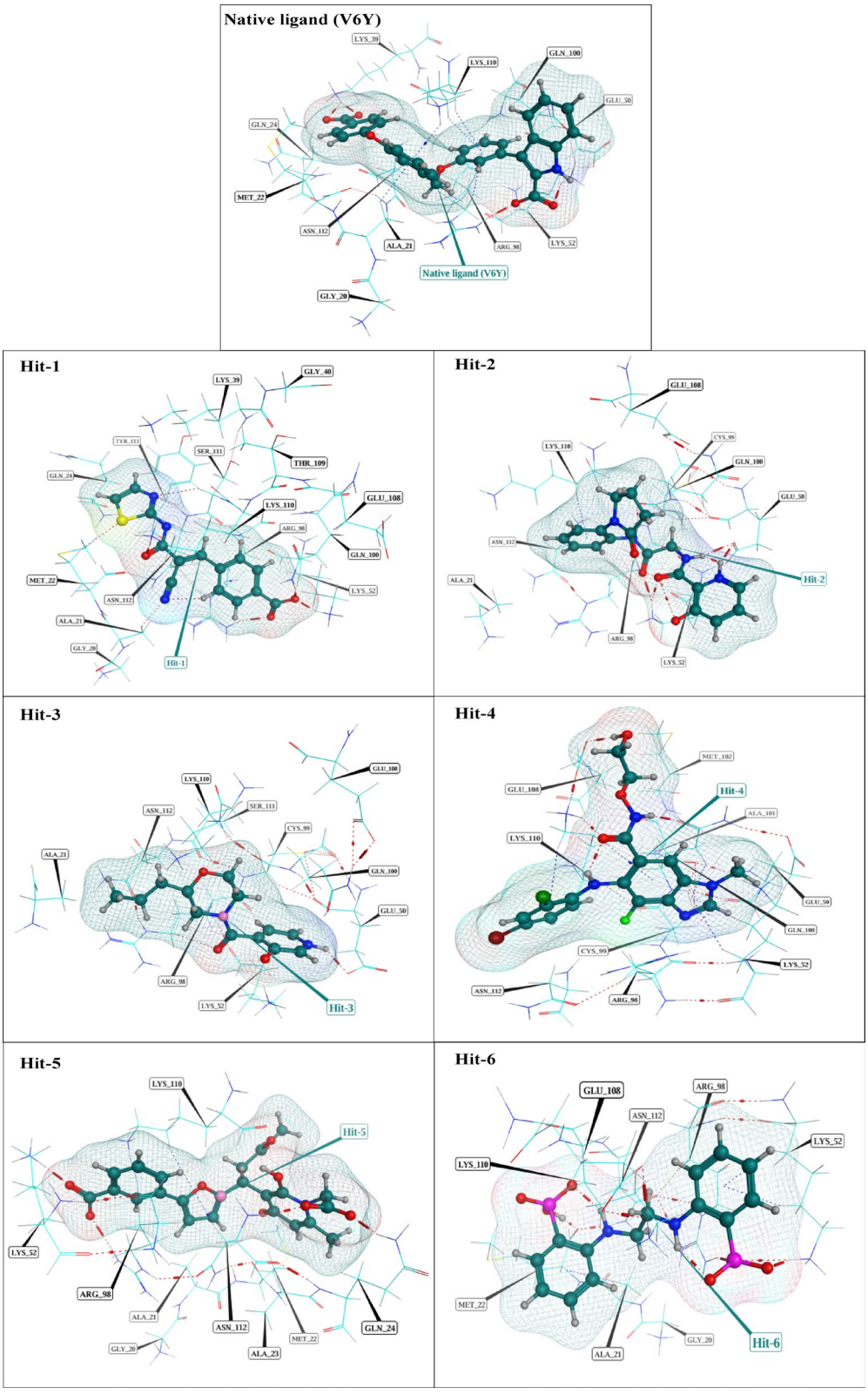

Fig. 1. 3D ligand interactions diagram of native ligand (V6Y) and the top six hit compounds with RAGE (PDB ID: 6XQ3). The protein residues are shown as light-blue lines and the ligand molecules are represented as a teal-colored ball and sticks model, the dotted red line indicates the H-bonds with backbone residues, whereas the dotted blue line represents H-pi bonds.

docked into the binding site of the RAGE protein. The docking scores of the screened hits ranged between − 5.116 kcal/mol for Hit-4 to − 10.008 kcal/mol for Hit-5 as compared to the native inhibitor − 7.033 kcal/mol. The lower docking score values illustrated the stable conformations of the receptor-ligand complexes. Among the top six selected compounds, the compound Hit-5 (− 10.008 kcal/mol) showed the best binding affinity followed by Hit-6 (− 9.109 kcal/mol), Hit-1 (− 8.109 kcal/mol), Hit-2 (− 7.074 kcal/mol) and Hit-3 (− 6.698 kcal/mol). However, the compound Hit-4 (− 5.116 kcal/mol) exhibited the least binding affinity.

The native inhibitor (V6Y) binds into the catalytic region of the VC1 domain of RAGE with a docking score of − 7.033 kcal/mol. It exhibits four hydrogen bonds (H-bonds) with amino acid residues LYS_39, LYS_52, ARG_98, and ASN_112. The receptor residues showed two salt bridges with LYS_39 and LYS_52 and one pi-cat interaction with LYS_110. Six compounds were selected after pose and interaction analysis due to their strong binding affinity and diverse residue interactions. In the top six complex systems, key residues such as MET_22, GLN_24, GLU_50, LYS_52, ARG_98, CYS_99, GLN_100, GLU_108, LYS_110, and ASN_112 were mainly involved in the hydrogen bonding interactions. Additionally, GLU_50, LYS_52, ARG_98, and LYS_110 amino acid residues contributed through salt bridges and pi-cat interactions with the ligands. LYS_52, ARG_98, and LYS_110 played a crucial role in these binding interactions by forming multiple bonds. Further, molecular dynamics simulations of the top six selected receptor-ligand poses were performed to verify the key interactions of the docking poses.

Molecular dynamics (MD) simulations

To validate the suitability and stability of the docked poses, the native inhibitor (V6Y) and six top-scored RAGE-ligand complexes were shortlisted and subjected to MD simulations for 100 ns in physiological environments with OPLS4 force field by utilizing the Desmond package of Schrodinger's Suite (Release 2024-1). The Root mean square deviation (RMSD) and root mean square fluctuation (RMSF) of the native inhibitor and the top six compounds were calculated and analyzed to examine the fluctuation of the two systems. Further, various intermolecular interactions (hydrogen bonds, hydrophobic, ionic, and water bridges), dynamic cross-correlation matrix (DCCM), and principal component analysis (PCA) were also performed to assess the MD trajectories at the residue level.

RMSD analysis

The stability of the standard inhibitor (V6Y) of the VC1 domain of the RAGE protein (PDB Id: 6XQ3) and top six complexes (a) Hit-1, (b) Hit-2, (c) Hit-3, (d) Hit-4, (e) Hit-5 and (f) Hit-6 was analyzed through the RMSD. The smaller RMSD value suggests a more stable protein structure and changes up to 1–3 Å are within the acceptable range, however, larger values may indicate that the protein is undergoing substantial conformational changes during simulation. The average RMSD values for C-alpha atoms of the protein across all complexes were: V6Y (2.295 Å), Hit-1 (3.440 Å), Hit-2 (4.153 Å), Hit-3 (3.155 Å), Hit-4 (2.354 Å), Hit-5 (2.793 Å), and Hit-6 (4.049 Å). The native ligand (V6Y) stabilizes after approximately 50–60 ns, indicating that the protein attains structural stability during the simulation. The Hit-2 shows elevated P-RMSD values, particularly after approximately 60 ns, suggesting considerable structural deviations and instability, which indicates it may not function as a strong binder and could compromise the protein's stability. Hit-4, Hit-5, and Hit-6 exhibited stable P-RMSD values comparable to the native ligand, indicating their capacity for effective binding without significant structural disruptions. Hit-1 and Hit-3 exhibit moderate P-RMSD fluctuations, indicating partial stability and warranting further investigation. The average L-RMSD values for the native inhibitor were recorded as follows: V6Y (3.250 Å), Hit-1 (7.987 Å), Hit-2 (3.774 Å), Hit-3 (3.466 Å), Hit-4 (2.699 Å), Hit-5 (4.544 Å), and Hit-6 (5.837 Å). Hit-2, Hit-3, and Hit-4 demonstrated minimal deviation, as indicated by their average L-RMSD values, while Hit-1, Hit-5, and Hit-6 showed significant alterations in average L-RMSD values relative to the native ligand.

The superimposition of the native inhibitor (V6Y in complex with RAGE) and all six simulated systems suggested that Hit-4, Hit-5, and Hit-6 behaved more stable followed by the reference compound as illustrated in Fig. 2a and b. The individual protein-ligand RMSD plots are presented in Supplementary Fig. S3. The simulation time was extended to 500 ns for the native ligand (V6Y), Hit-5, and Hit-6 compounds. The results indicated that the protein RMSD of the Hit-6 complex improved, positioning it as an ideal lead molecule, as shown in Supplementary Fig. S4.

RMSF analysis

The RMSF is an important parameter to understand the flexibility of each amino acid residue of the receptor over the simulation period. Generally, the secondary structure elements (alpha helices and beta strands) are stiffer and fluctuate less than their unstructured loop regions. Whereas, the C- and N-termini of the protein exhibit the majority of the variations. Changes up to 2 Å in the RMSF values of the protein-ligand interaction are considerably acceptable. The average P-RMSF values for the native inhibitor were recorded as follows: V6Y (1.422 Å), Hit-1 (1.578 Å), Hit-2 (2.608 Å), Hit-3 (1.404 Å), Hit-4 (1.745 Å), Hit-5 (1.671 Å), and Hit-6 (1.659 Å). The P-RMSF analysis plots indicated that the reference compound of the RAGE receptor, V6Y, exhibits peaks around residues 25, 80, 150–160, and 200–220, which correspond to flexible regions. The Hit-2 exhibited notable fluctuations in various regions, particularly in the terminal and loop regions, suggesting that this ligand induces considerable flexibility in the protein, indicative of weak or unfavourable interactions. Hit-1 and Hit-3 demonstrated low RMSF values comparable to the native ligand, indicating their capacity to preserve protein stability and induce minimal structural fluctuations. Conversely, Hit-4, Hit-5, and Hit-6 exhibited moderate flexibility and may necessitate additional investigation.

To conclude, the superimposed trajectories of the native inhibitor and the top six simulated systems depicted that all the complexes showed comparable PL-RMSF values except Hit-1 and Hit-2 suggesting that these complexes were as stable as the reference compound (V6Y) as plotted in Fig. 3a and b. Similarly, Supplementary

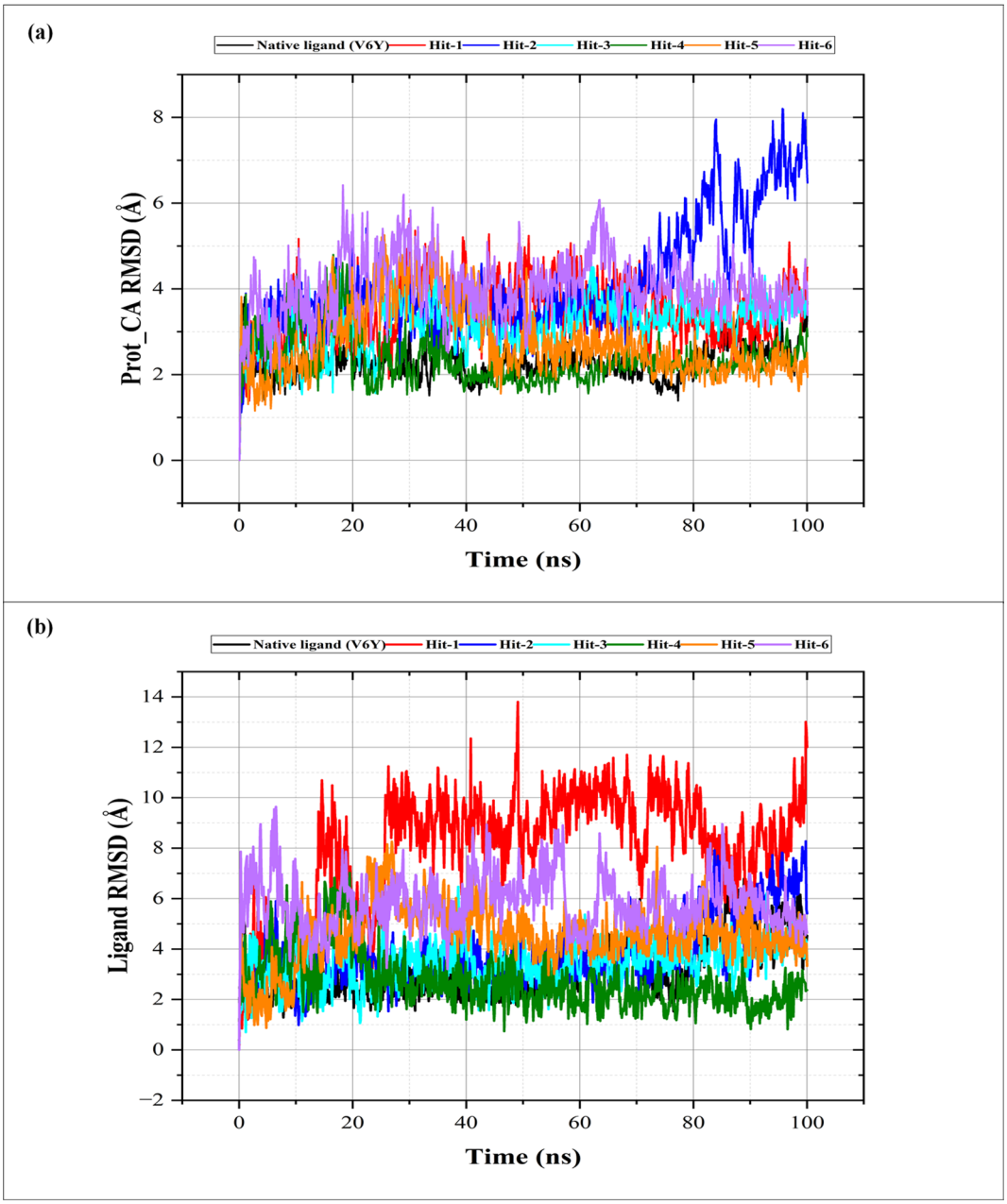

Fig. 2. Protein-ligand RMSD plot of the native ligand (V6Y) and the top six hit compounds over 100 ns trajectory (**a**) Time-dependent RMSD values for C-alpha atoms of the protein, and (**b**) ligand RMSD values. The P-RMSD values of most systems stabilize after approximately 20–40 ns, indicating that the protein backbone achieves equilibrium within this period.

Figure S5 displays the P-RMSF plot and Supplementary Figure S6 displays the L-RMSF plot. Also, Supplementary Fig. S7 shows the findings of the extended simulations of the natural ligand (V6Y), Hit-5, and Hit-6 compounds along a 500 ns trajectory.

Protein-ligand contacts

The protein-ligand contact histogram depicts all interaction types during the 100 ns simulation run. The interactions between the protein and the chosen compounds are influenced by various interactions (or 'contacts') including hydrogen bonds, hydrophobic interactions, ionic bonds, and water bridges. The protein-ligand contact histogram revealed that the native ligand (V6Y) formed H-bond interactions with various amino acid residues of RAGE such as GLY_20, GLN_24, LYS_39, LYS_52, ARG_98, GLN_100, LYS_107, LYS_110, SER_111, ASN_112, and ARG_198 while hydrophobic interactions with GLY_20, ALA_21, MET_22, LYS_52, ARG_98, LYS_107 and LYS_110. Formation of ionic interactions with amino acid residues GLY_20, LYS_39, LYS_52, ARG_98, GLN_100, LYS_107, LYS_110, and ARG_198 depicted strong affinity of V6Y with RAGE.

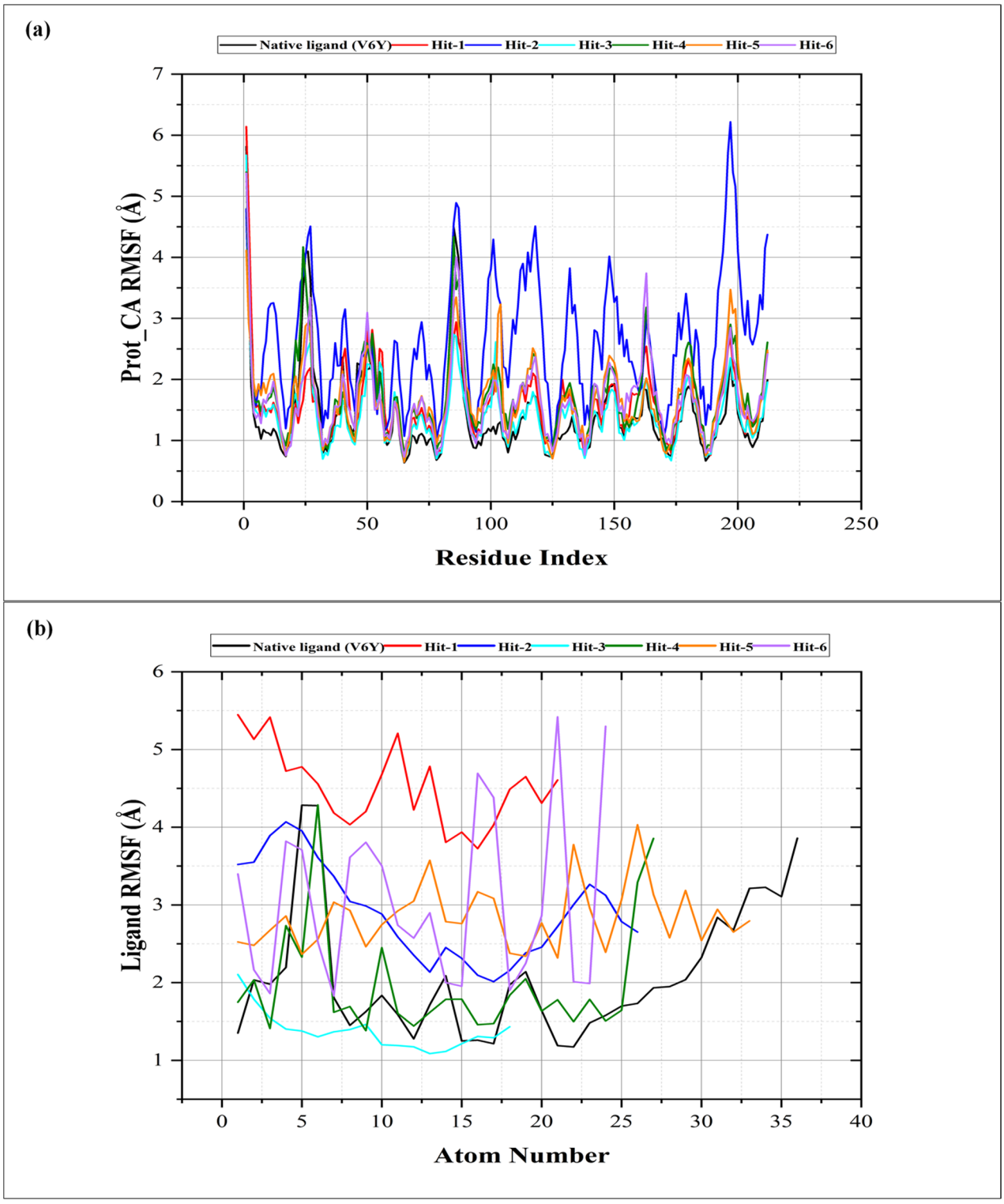

Fig. 3. Protein–ligand RMSF plot of the native ligand (V6Y) and the top six hit compounds over 100 ns trajectory (**a**) RMSF values for C-alpha atoms of the protein across residue indices, and (**b**) ligand RMSF values. Peaks around residues 25, 80, 150–160, and 200–220 correspond to flexible regions.

In addition, it also established several water bridge interactions with GLY_20, ALA_21, MET_22, ALA_23, GLN_24, LYS_39, ARG_48, GLU_50, LYS_52, ARG_98, GLN_100, LYS_107, GLU_108, THR_109, LYS_110, SER_111, ASN_112, TYR_113 and ARG_198 signifying its ability to inhibit the RAGE receptor (Fig. 4a).

Likewise, the protein-ligand (PL) contacts of the top six selected complexes (a) Hit-1, (b) Hit-2, (c) Hit-3, (d) Hit-4, (e) Hit-5, and (f) Hit-6 were also monitored over 100 ns simulation time. Protein-ligand contacts

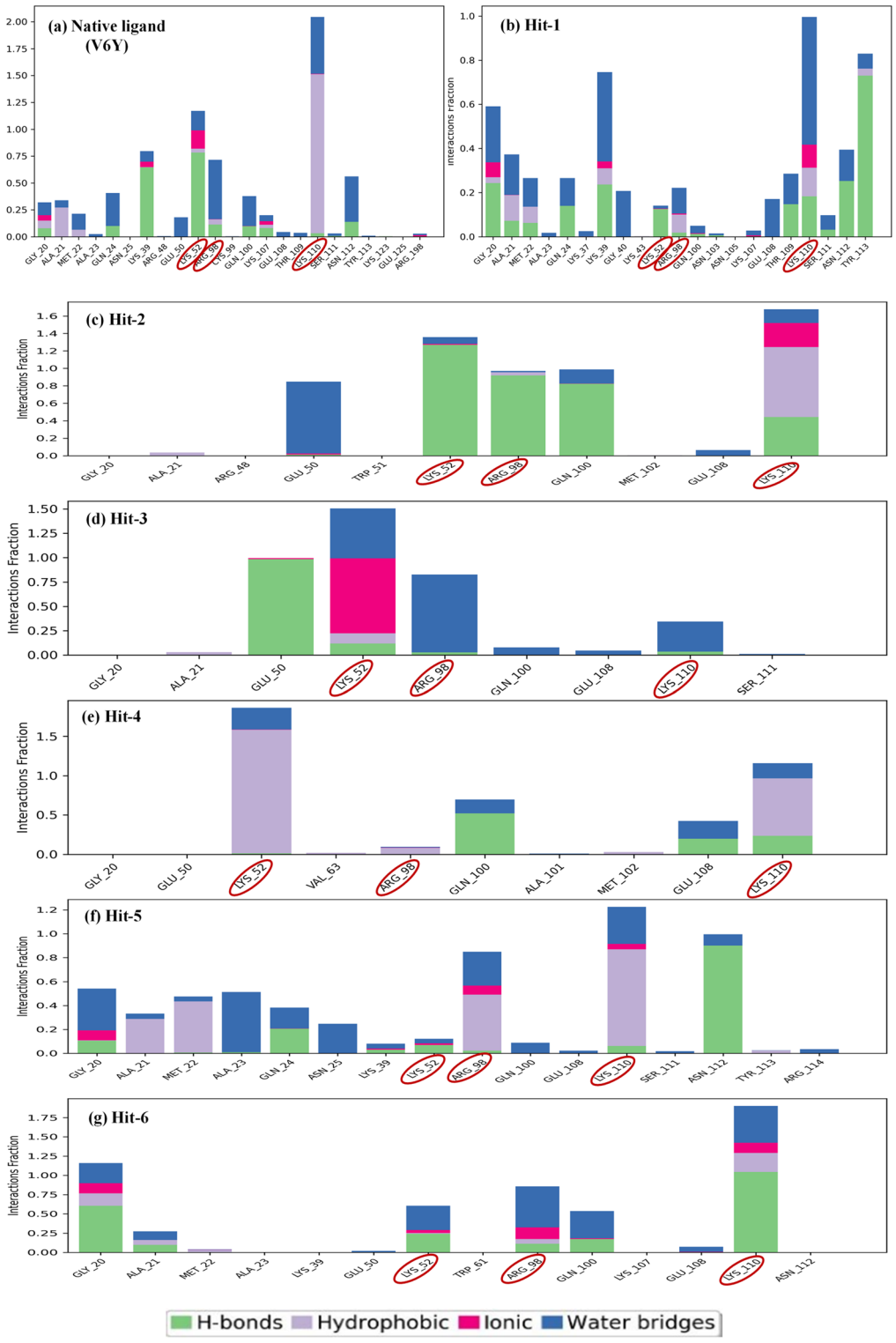

Fig. 4. Protein–ligand contact histogram of the native ligand (V6Y) and the top six hit compounds. The conserved amino acid triad (LYS_52, ARG_98, and LYS_110) is highlighted in red.

that maintained an interaction of 10% or greater simulation time have been deliberated further. Even though hydrogen and hydrophobic interactions are weaker than ionic bonds, they play a crucial role in developing novel drug candidates.

MD simulation trajectory revealed that the Hit-1 compound formed several hydrogen bonding interactions with GLY_20, GLN_24, LYS_39, LYS_52, THR_109, LYS_110, ASN_112, and TYR_113 while hydrophobic interactions with ALA_21, ARG_98, and LYS_110. Moreover, it also forms ionic bond interactions with the

amino acid residues GLY_20 and LYS_110 and water bridges with GLY_20, ALA_21, MET_22, GLN_24, LYS_39, GLY_40, ARG_98, GLU_108, THR_109, LYS_110, and ASN_112 (Fig. 4b).

The simulation interaction of the Hit-2 compound showed H-bonds with LYS_52, ARG_98, GLN_100, and LYS_110 whereas it forms hydrophobic interaction with LYS_110 amino acid residue. In addition, it also established ionic interaction with LYS_110 and water bridges with GLU_50, GLN_100, and LYS_110 (Fig. 4c).

Similarly, GLU_50 and LYS_52 amino acid residues play a crucial role in Hit-3 docked complex stability via hydrogen bonding interaction. Moreover, hydrophobic interaction with LYS_52 was well maintained. In addition, the Hit-3 compound shows the formation of one ionic bond with LYS_52 and several water bridge interactions with LYS_52, ARG_98, and LYS_110 providing additional stability to the complex (Fig. 4d).

On the other hand, the Hit-4 compound interacted with several amino acid residues such as GLN_100, GLU_108, and LYS_110 by forming hydrogen bond interactions along with LYS_52 and LYS_110 by forming hydrophobic interactions. Furthermore, it also forms water bridges with LYS_52, ARG_98, and LYS_110 that provide stability to the complex (Fig. 4e).

The Hit-5 compound formed H-bond interactions with GLY_20, GLN_24, LYS_52, and ASN_112 whereas hydrophobic interactions with the amino acid residues ALA_21, MET_22, ARG_98, and LYS_110. In addition, GLY_20, ARG_98, and LYS_110 residues play a key role in the binding process through ionic bond formation whereas it also forms several water bridges with GLY_20, ALA_23, GLN_24, ASN_25, ARG_98, GLN_100, LYS_110, and ASN_112 (Fig. 4f).

Additionally, the MD trajectory of the Hit-6 compound showed H-bond interactions with GLY_20, ALA_21, LYS_52, ARG_98, GLN_100, and LYS_110 whereas hydrophobic interactions with GLY_20 and LYS_110. Correspondingly, the Hit-6 compound shows the formation of ionic bond interaction with GLY_20, ARG_98, and LYS_110 and numerous water bridge interactions with GLY_20, LYS_52, ARG_98, GLN_100, and LYS_110 (Fig. 4g).

To conclude, the GLY_20, GLU_50, LYS_52, ARG_98, LYS_110, ASN_112, and TYR_113 residues played crucial roles in the binding process via hydrogen bonding interactions amongst all the hit compounds. Correspondingly, the residues LYS_52, ARG_98, and LYS_110 provide stability by forming ionic bonds. Hit-4 and Hit-5 formed strong hydrophobic interactions and water bridges. The Hit-6 compound showed multiple ionic and hydrogen bonds, suggesting it could be a potential lead molecule for inhibiting the RAGE enzyme.

Dynamic cross-correlation map (DCCM)

The DCCM analysis is a common technique for examining structural differences through MD simulation trajectories of the protein-ligand complexes. The DCCM calculates correlation coefficients based on the system's interconnected fluctuations[32]. The cross-correlation matrix provides information about the correlated and anti-correlated motions between residues. The DCCM shows the correlation of atomic displacements in residues, ranging from −1 to +1, where +1 represents a positive correlation while −1 shows a negative correlation. The densely colored sections demonstrate a positive correlation (represented in blue) and a negative correlation (represented in red) between protein residues. In contrast, the uncolored regions indicate no correlation in residue mobility[33]. Positive correlation means two residues tend to move in the same direction and the intensity of the color indicates the strength of the correlation. For example, a brighter blue color indicates a stronger positive correlation and the same will apply to the negative correlation. The DCCM results revealed that Region-1 (residues 20–70) is indicated by a red box, highlighting the synchronised movement of the residues. Hit-1, Hit-4, and Hit-6 exhibit a strong positive correlation in their motions when compared to the native ligand (V6Y) and other hits, indicating more coordinated movements. In region-2 (residues 90–125), indicated by the yellow box, anticorrelated motions were noted in the native ligand (V6Y), Hit-1, Hit-3, Hit-4, and Hit-5. In contrast, Hit-6 and Hit-2 exhibited relatively fewer negatively correlated motions. The data indicates that all the hits exhibit more distinct correlations and anti-correlations compared to the native ligand (V6Y). This distinction is essential for the stability of the system and the functional movements of active site residues, particularly the triad residues: LYS_52, ARG_98, and LYS_110, as illustrated in Supplementary Fig. S8.

Principal component analysis (PCA)

The PCA is a popular statistical technique used to better understand the dynamic behavior of biological systems. It considers the trajectory of an MD simulation and simplifies the dimensionality and complexity of the data to easily compare and identify differences in motions between wild-type and mutants[34]. The first principal component (PC1) is the line or score representing the data's highest variance direction. The second principal component (PC2) aligns with the second significant source of variation in the data and is perpendicular to the PC1.

PCA analysis depicts the induced conformational dynamics of the native ligand (V6Y) along with the top six lead compound complexes i.e., Hit-1, Hit-2, Hit-3, Hit-4, Hit-5, and Hit-6. Densely clustered points represent similar conformations, implying that the system remained stable or experienced minor changes over the simulation time. In contrast, more dispersed areas on the plot characterize higher structural diversity, indicating regions with strong conformational flexibility. The results demonstrated that Hit-1, Hit-3, and Hit-4 exhibit moderate deviation from the native ligand cluster, indicating distinct conformations relative to the native ligand (V6Y). Hit-2 exhibits a greater divergence from the native cluster and does not coincide with the native conformational state. Hit-5 and Hit-6 exhibit closely overlapping points with the native cluster, suggesting significant conformational and structural stability. Various clusters were depicted using distinct colours and shapes, as illustrated in Supplementary Fig. S9.

MM-GBSA free energy calculations

The post-simulation binding free energies of the selected protein-ligand complexes were determined using the Prime MM-GBSA approach of the Schrodinger's package (Release 2024-1). The predicted binding free energy of the co-crystallized ligand (V6Y) was found to be -43.246 kcal/mol and set as the benchmark cut-off score for identifying novel inhibitors of the RAGE receptor. Similarly, the calculated binding energy for the hit compounds ranged between − 32.084 kcal/mol to − 48.487 kcal/mol. The Hit-4 compound exhibited the lowest binding free energy value of − 48.487 kcal/mol followed by the Hit-5 compound with a ΔG_{Bind} value of -47.941 kcal/mol compared to the other hit compounds depicting that Hit-4 and Hit-5 bind more tightly to the RAGE receptor. However, the Hit-6 compound displayed an extraordinary $\Delta G_{Coulomb}$ (Electrostatic Coulomb) value of -268.458 kcal/mol compared to the native ligand (− 197.004 kcal/mol) demonstrating that Hit-6 also binds more tightly compared to the RAGE protein than the other hit compounds. The essential binding energy values for the native ligand and the top six hit compounds over a 100 ns trajectory were presented in Table 2. The binding energy terms for the FDA-approved drugs over a 100 ns trajectory were given in Supplementary Table S3. The binding energy terms for the native ligand, Hit-5, and Hit-6 over a 500 ns trajectory were shown in Supplementary Table S4. The comprehensive MM-GBSA results were provided in Supplementary Tables S5-S7. A precise comparison of docking energy and binding energy is presented in Supplementary Fig. S10a, while the average ΔGBind (in kcal/mol) between the original inhibitor and the top six screened compounds is shown in Supplementary Fig. S10b.

Per-residue decomposition analysis

The analysis of residue decomposition was conducted using the breakdown_MMGBSA_by_residue.py script included in the Prime module of the Schrodinger suite (Release 2024-1). This study analyses decomposition energies derived from binding energy calculations, highlighting the contribution of individual amino acid residues. The key amino acid residues LYS_52, ARG_98, and LYS_110 exhibited a consistent binding pattern in RAGE and its associated ligands. The compounds Hit-1, Hit-2, Hit-3, Hit-4, Hit-5, and Hit-6 exhibited comparable key residues to the native ligand (V6Y), indicating the stability of these complexes.

The energy decomposition analysis revealed significant residues that substantially influence the overall interaction energy. The decomposition analysis identified a minimum of 10 amino acid residues, specifically GLY_20, ALA_21, LYS_39, GLU_50, LYS_52, ARG_98, GLN_100, LYS_110, ASN_112, and ARG_198, that significantly contribute to protein-ligand interactions. In the reference compound (V6Y), ARG_98 contributes − 7.41 kcal/mol to the binding free energy through hydrogen bonding, hydrophobic interactions, and coulombic interactions. In a similar manner, the residues GLY_20, ALA_21, LYS_39, GLU_50, LYS_52, GLN_100, LYS_110, ASN_112, and ARG_198 exhibited interaction energies ranging from − 0.06 to − 5.66 kcal/mol. The interaction of Hit-1 with the target receptor was enhanced by various amino acid residues, with contributions ranging from − 1.82 kcal/mol (LYS_39 through hydrogen bonding, Van der Waals, and Coulombic interactions) to 0.32 kcal/mol (GLU_50 via solvation and Van der Waals forces). In the case of Hit-2, the energy contribution of ARG_98 was recorded at − 9.37 kcal/mol, indicating high activity, attributed to coulombic interactions, hydrogen bonding, and hydrophobic interactions including van der Waals, lipophilic, and pi-pi interactions. Conversely, GLU_50 exhibited minimal significance with an energy contribution of 0.24 kcal/mol, associated with coulombic, lipophilic, and van der Waals interactions. Residue ARG_98 significantly contributes to the binding of the Hit-3 compound through coulombic, van der Waals, hydrogen bonding, and lipophilic interactions, exhibiting a binding energy of − 5.08 kcal/mol, indicating high activity. In contrast, the energy contribution of LYS_39 is 0.05 kcal/mol, reflecting lower activity, primarily through coulombic and van der Waals forces. The interaction of the Hit-4 compound with the target receptor was significantly facilitated by GLN_100, exhibiting an energy contribution of − 6.68 kcal/mol, attributed to coulombic interactions, hydrogen bonding, and hydrophobic interactions, including van der Waals, lipophilic, and pi-pi interactions. In contrast, GLY_20 demonstrated minimal activity, with an energy contribution of 0.18 kcal/mol, resulting from coulombic, van der Waals, and lipophilic interactions. In the context of Hit-5, the energy contribution of the ASN_112 residue was determined to be − 3.82 kcal/mol, indicating high activity, due to the formation of coulombic interactions, hydrogen bonding, and hydrophobic interactions, including van der Waals, lipophilic, and pi–pi interactions.

S. no.	Ligand	ΔG_{Bind}	$\Delta G_{Coulomb}$	$\Delta G_{Covalent}$	ΔG_{Hbond}	ΔG_{Lipo}	ΔG_{SolvGB}	ΔG_{vdW}
1.	Native ligand (V6Y)	− 43.246	− 197.004	− 1.725	− 2.754	− 4.601	198.944	− 33.173
2.	Hit-1	− 32.084	− 171.983	1.501	− 2.142	− 5.653	174.268	− 26.657
3.	Hit-2	− 40.352	− 47.817	2.273	− 2.263	− 5.404	48.252	− 32.624
4.	Hit-3	− 35.544	− 33.699	0.448	− 0.850	− 5.440	36.736	− 31.808
5.	Hit-4	− 48.487	− 23.337	1.944	− 1.031	− 8.467	24.713	− 38.616
6.	Hit-5	− 47.941	− 162.266	0.871	− 1.375	− 8.828	165.293	− 39.157
7.	Hit-6	− 42.225	− 268.458	1.811	− 3.019	− 5.750	260.820	− 25.578

Table 2. MM-GBSA values for the native ligand (V6Y) and the top six hit compounds (in kcal/mol). ΔG_{Bind}: Total binding free energy averaged over the simulation time; $\Delta G_{Coulomb}$: Electrostatic Coulomb term of the binding energy; $\Delta G_{Covalent}$: Covalent term of the binding energy; ΔG_{Hbond}: Hydrogen bond contribution to the binding energy; ΔG_{Lipo}: Lipophilic contribution to the binding energy; ΔG_{SolvGB}: Generalized Born term of the solvation energy; ΔG_{vdW}: van der Waals term of the binding energy.

Conversely, the energy contribution of GLU_50 was measured at 0.31 kcal/mol, reflecting low activity, primarily through solvation and van der Waals forces. The interaction of the Hit-6 compound with the target receptor was significantly enhanced by residues ARG_98, which engaged in coulombic interactions, hydrogen bonding, and hydrophobic interactions, including van der Waals, lipophilic, and pi-pi interactions. LYS_110 contributed through coulombic, van der Waals forces, and hydrogen bonding, with energy contributions of -6.68 kcal/mol and − 6.27 kcal/mol, respectively. In contrast, GLU_50 exhibited the least activity, with an energy contribution of 0.76 kcal/mol, attributed to solvation and van der Waals forces.

Complexes containing the residues GLY_20, ALA_21, LYS_39, GLU_50, LYS_52, ARG_98, GLN_100, LYS_110, ASN_112, and ARG_198 demonstrate significant stability and binding strength, as depicted in Supplementary Fig. S11. The comprehensive energy distribution of all amino acid residues, heteroatoms, and the ligand molecule (UNK) for the native inhibitor, top-six hit compounds, and FDA-approved drugs over a 100 ns trajectory is presented in Supplementary Table S8 and Supplementary Table S9, respectively. The energy distribution of the native ligand, Hit-5, and Hit-6 over a 500 ns trajectory is presented in Supplementary Table S10.

In- silico ADME and toxicity prediction

The pharmacokinetic properties of the native inhibitor (V6Y) and the top six hit compounds were evaluated based on their physicochemical, drug-likeliness, medicinal chemistry, and toxicity using the ADMETLab 2.0 web tool. The compounds were screened based on various parameters such as molecular weight (MW), topological polar surface area (TPSA), no. of rotational bonds (nRot), octanol-water partition coefficient (logP), aqueous solubility (logS), Lipinski's rule of five, Pan Assay Interference Compounds (PAINS), the permeability of Caco-2 cells (Caco-2), the permeability of MDCK cells (MDCK), human intestinal absorption (HIA), blood-brain barrier penetration (BBB), plasma-protein binding (PPB), CYP 2D6 inhibitor/substrate, clearance of the drug (CL), the half-life of the drug ($T_{1/2}$), HERG K^+ channel blockage prediction (hERG), AMES toxicity, skin sensitization, and Carcinogenicity. The important ADMET parameters of the native inhibitor and the top six hit compounds have been provided in Table 3. The complete ADMET table is provided in Supplementary Table S11.

Predicting the physicochemical properties is a crucial step in the development of a molecule to become a potent lead molecule. ADMETLab 2.0 results showed that the molecular weights of all the hit compounds were within the recommended range i.e., 100–600 g/mol. The topological polar surface area (TPSA) values of all the compounds preferably lie in the range of (0-140 Å) except for Hit-5. The number of rotational bonds for all the compounds was in the acceptable range (0–11). The log P values of all the compounds were within the range of 0–3 log mol/L except the compound Hit-4. Similarly, the log S values of the compounds lie in the range of − 4 to 0.5 log mol/L except for the compound Hit-4.

There were zero violations of Lipinski's rule of five, and no alerts in the PAINS investigation for all the hit compounds. In addition, MDCK and Caco2 cell permeability values of the compounds preferably lie in the range of greater than or equal to 2×10^{-6} cm/s and greater than or equal to − 5.15 log cm/s respectively. The Hit-2, Hit-4, and Hit-5 compounds showed excellent human intestinal absorption (HIA) values, Hit-3 showed medium HIA, whereas Hit-1 and Hit-6 displayed alerts.

Furthermore, Hit-1, Hit-5, and Hit-6 compounds exhibited excellent blood-brain-barrier (BBB) permeability values of 0.199, 0.016, and 0.226 respectively, and Hit-4 showed medium BBB values of 0.307, however, Hit-2 and Hit-3 showed alerts with values of 0.834 and 0.875 respectively. Out of six-hit compounds, four compounds (Hit-1, Hit-2, Hit-3, and Hit-6) with excellent plasma protein binding (PPB) values i.e., less than or equal to 90% were considered to have a proper PPB, and the rest of the compounds (Hit-4 and Hit-5) with high protein-bound may have a low therapeutic index. The inhibition of the CYP 2D6 inhibitor/substrate for all the compounds was predicted within the range of 0-0.3 except for the Hit-3 compound, which exhibited a slightly higher value of CYP 2D6 substrate (0.336), where the output value is the probability of being substrate/ inhibitor. The clearance of a drug is an important factor that defines the volume of distribution, the half-life, and the frequency of drug dosage. The results revealed that Hit-4 showed excellent clearance whereas the remaining compounds illustrated poor clearance. In addition, the half-life of all the compounds was also predicted, Hit-2, Hit-3, and Hit-4 compounds showed medium $T_{1/2}$ values among the other hits.

The prediction of toxicological parameters is an important step in the drug discovery process since most of the potential lead compounds fail due to their toxicity. Consequently, the selected compounds were also evaluated based on their toxicological behavior. The predicted IC_{50} value for blockage of $HERG^+$ channels (hERG) criteria was satisfied by all the hit compounds within the recommended range i.e., 0-0.3. Moreover, except for Hit-1, the other compounds resulted in negative AMES toxicity i.e., representing their non-carcinogenic behavior. The Hit-5 compound resulted in negative skin sensitization as compared to other compounds. Furthermore, the Hit-2, Hit-5, and Hit-6 compounds showed negative carcinogenicity i.e., denoting their non-carcinogenic behavior except for other hit compounds. Overall Hit-5 and Hit-6 showed 62 excellent properties out of 88 ADMET parameters as compared to other hit compounds suggesting that these two compounds could be potential inhibitors of RAGE. Furthermore, the Hit-6 compound exhibited the selective ADMET parameters that are important for a lead compound to possess neurological properties.

Discussion

Alzheimer's Disease (AD) is a complicated, multifaceted neurodegenerative disorder that causes dementia and progressive cognitive impairment due to brain cell death[35,36]. It is characterized by the accumulation of senile plaques, containing neurotoxic amyloid-beta (Aβ) and neurofibrillary tangles, with abnormally activated tau (τ) protein[9,37]. Although there is no cure for AD, certain treatments may alter the disease's development, and both medications and non-drug approaches can assist in managing symptoms. It is believed that the extensive occurrence of RAGE-related neuroinflammation in AD, the link between inflammation and the severity of AD,

S. no.	Ligand	Physicochemical properties					Medicinal chemistry		Absorption			Distribution		Metabolism		Excretion		Toxicity			
		MW	TPSA	nRot	logP	logS	Lipinski Rule	PAINS	Caco-2	MDCK	HIA	BBB	PPB	CYP2D6-inh	CYP2D6-sub	CL	$T_{1/2}$	hERG	Ames Toxicity	SkinSen	Carcinogenicity
1.	V6Y (Native)	479.14	108.85	8	5.903	− 3.039	Accepted	0	− 5.587	6.57E−06	0.08	0.052	102.12%	0.191	0.04	0.464	0.643	0.531	0.026	0.02	0.763
2.	Hit-1	299.04	106.31	4	2.229	− 3.517	Accepted	0	− 5.588	2.05E−05	0.768	0.119	82.72%	0.024	0.107	2.698	0.923	0.046	0.984	0.859	0.725
3.	Hit-2	354.13	111.63	7	0.626	− 3.29	Accepted	0	− 5.043	9.24E−06	0.295	0.834	59.64%	0.037	0.234	4.378	0.641	0.049	0.027	0.396	0.043
4.	Hit-3	250.13	62.66	4	1.377	− 1.054	Accepted	0	− 4.527	1.10E−05	0.527	0.875	29.34%	0.021	0.336	3.402	0.499	0.042	0.137	0.853	0.31
5.	Hit-4	456	88.41	7	4.176	− 5.852	Accepted	0	− 4.542	2.15E−05	0.007	0.307	96.66%	0.016	0.163	6.154	0.531	0.041	0.389	0.37	0.732
6.	Hit-5	455.12	156.27	9	2.528	− 3.584	Accepted	0	− 5.743	2.56E−05	0.16	0.016	95.24%	0.019	0.101	1.197	0.905	0.03	0.009	0.025	0.096
7.	Hit-6	372.06	132.8	7	0.085	− 2.321	Accepted	0	− 6.073	9.22E−06	0.999	0.226	66.22%	0.014	0.106	1.74	0.9	0.004	0.037	0.914	0.007

Table 3. ADMET properties of the native ligand (V6Y) and the top six hit compounds. Recommended range: MW (Molecular Weight): 100–600 g/mol; TPSA (Topological polar surface area): 0-140; nRot (Number of Rotatable Bonds): 0–11; logP (Logarithm of n-octanal/water distribution coefficient): 0–3 mol/L; logS (Logarithm of aqueous solubility): − 4 to 0.5 mol/L; Lipinski's Rule: MW ≤ 500; logP ≤ 5; Hacc ≤ 10; Hdon ≤ 5; PAINS (Pan Assay Interference Compounds): Frequent hitters, alpha-screen artifacts and reactive compounds; Caco-2 Permeability: > − 5.15: Excellent (green); otherwise: Poor (red) ; MDCK Permeability: $> 2 \times 10^{-6}$ cm/s: Excellent (green); otherwise: Poor (red); HIA (Human Intestinal Absorption): 0–0.3: Excellent (green); 0.3–0.7: Medium (yellow); 0.7–1.0 (++) Poor (red); BBB Penetration (Blood-brain barrier): 0–0.3: Excellent (green); 0.3–0.7: Medium (yellow); 0.7–1.0 (++) Poor (red); PPB (Plasma protein binding): ≤ 90%: excellent (green); otherwise: poor (red); CYP 2D6 inhibitor/ substrate: Category 0: Non-inhibitor; Category 1: inhibitor (Probability of being substrate within 0–1(grey)) ; CL (Clearance): ≥ 5: Excellent (green); < 5: Poor (red); $T_{1/2}$ (Half-life): 0–0.3: Excellent (green); 0.3–0.7: Medium (yellow); 0.7–1.0 (++) Poor (red); hERG Blockers (Human ether-a-go-go gene): 0–0.3: Excellent (green); 0.3–0.7: Medium (yellow); 0.7–1.0 (++) Poor (red); AMES Toxicity: 0–0.3: Excellent (green); 0.3–0.7: Medium (yellow); 0.7–1.0 (++) Poor (red); Skin Sensitization: 0–0.3: Excellent (green); 0.3–0.7: Medium (yellow); 0.7–1.0 (++) Poor (red); Carcinogenicity: 0–0.3: Excellent (green); 0.3–0.7: Medium (yellow); 0.7–1.0 (++) Poor (red).

and the rise in inflammatory markers in the AD brain all suggest that RAGE-driven inflammation is crucial in advancing the disease[38].

RAGE is a multi-ligand receptor and can bind to multiple extracellular and intracellular ligands such as AGEs, S100 calcium-binding proteins, amyloid-β, and HMGB1, etc. due to the presence of different domains (V, C1, and C2)[39–41]. The binding of RAGE to its ligands activates nuclear factor kappa B (NF-κB) through multiple signaling pathways including ERK, STAT3, MAPK, and JNK[42,43]. Several RAGE inhibitors such as Azeliragon, FPS-ZM1, and its fluorine-18 analog showed promising results and have the potential to act as effective antagonists against RAGE. However, most of them are in preclinical trials and more human clinical trials must be conducted to confirm their safety and effectiveness for treating numerous RAGE-related disorders[44–46]. Further, to establish potential targeted RAGE therapeutic approaches, future investigations are required to understand the efficacy of RAGE-targeting therapies and the long-term effects of RAGE blockade in humans.

This study conducted structure-based virtual screening utilizing various chemical libraries via SP and XP docking with the receptor grid of the minimised RAGE protein (PDB Id: 6XQ3), yielding 7114 XP hits. The assessment of ADME/T parameters was additionally conducted for the chosen top six hit compounds. The compounds underwent screening according to eighty-eight properties provided by the ADMETLab 2.0 webserver. The compounds exhibited consistent values across multiple categories, including physicochemical properties (17), medicinal chemistry (13), absorption (7), distribution (4), metabolism (10), excretion (2), toxicity (27), and 8 toxicophore rules. In the design of Alzheimer's disease-specific drugs, several ADMET properties are essential for ensuring both effectiveness and safety. These properties include blood-brain barrier (BBB) penetration, absorption and bioavailability, metabolism, half-life, distribution volume, toxicity, excretion, and interaction with P-glycoprotein (P-gp). The ADMET results indicated that the six highest predicted hit compounds, namely Hit-1, Hit-2, Hit-3, Hit-4, Hit-5, and Hit-6, demonstrated favourable hERG values, suggesting their potential to inhibit hERG protein and indicating a low risk of cardiac toxicity. All the hit compounds exhibited notable MDCK and Caco-2 values, indicating their low toxicity to the kidneys and intestines, respectively. The anti-cancer activity of the top six selected hits and the reference molecule was also predicted. The Hit-2, Hit-5, and Hit-6 compounds exhibited non-carcinogenic properties, while the co-crystallized ligand (V6Y), Hit-1, and Hit-4 displayed carcinogenic characteristics.

In addition, flexible docking analysis, such as IFD and MD simulations were accomplished to illustrate the stability of the complexes. The RAGE inhibition action of the top six hit compounds was predicted by utilizing molecular docking studies. The docking scores of the top six compounds ranged between − 5.116 to − 10.008 kcal/mol, comparable to the native inhibitor (− 7.033 kcal/mol). Based on the IFD results, the compound Hit-5 was the most active compound with a docking score of − 10.008 kcal/mol and established four hydrogen bonding interactions (GLN_24, LYS_52, ARG_98, and ASN_112) along with two salt bridges (LYS_52 and LYS_110), and one pi-cat interaction (LYS_110). Similarly, the Hit-6 compound showed the second-best docking score (− 9.109 kcal/mol) and formed three hydrogen bonds (MET_22, LYS_52, and ARG_98), and three salt bridges (LYS_52, ARG_98, LYS_110). In contrast, the Hit-4 molecule showed the least binding affinity (− 5.116 kcal/mol) and interacted with GLN_100 and GLU_108 by forming two hydrogen bonds and one pi-cat interaction with ARG_98.

Since the docking studies cannot imitate the body's receptor-ligand environment, MD simulations were performed for the top six molecules for 100 ns. The MD simulation results depicted better receptor-ligand interactions through the RMSD, RMSF, protein-ligand contacts, DCCM, and PCA plots. The RMSD plots remained consistent throughout the simulations, indicating the system's stability. The protein-ligand RMSD plot of the most active compound (Hit-6) showed fewer variations compared to the least active compound (Hit-4). The P-RMSF plot depicted the local fluctuations along the protein chain in the presence of ligands. At the same time, the L-RMSF signifies the ligand's atom-wise fluctuations, corresponding to its 2D structure. The P-RMSF values of the native ligand (V6Y) and the top six compounds except the Hit-2 were within the recommended range i.e., ~ 2 Å signifying that the systems were stable. The L-RMSF values suggested that the Hit-1 compound showed maximum fluctuations (4.520 Å) compared to other compounds. In addition, the protein-ligand histogram depicted various interactions such as hydrogen bonds, hydrophobic interactions, ionic bonds, and water bridges accomplished during the 100 ns simulation run. The top six screened compounds, Hit-1, Hit-2, Hit-3, Hit-4, Hit-5, and Hit-6 formed noticeably crucial interactions similar to the native compound (V6Y) and could be a potential lead candidate to inhibit target receptor RAGE. The structural differences among the top six systems were investigated through a dynamic cross-correlation map (DCCM). The results revealed that all six systems except Hit-2 exhibited moderate correlation and anti-correlation than the native inhibitor, whereas the Hit-2 compound displayed very high correlated and anti-correlated motions compared to the native ligand. Further, the PCA analysis displayed the conformational dynamics of the six systems along with the co-crystallized ligand. The PCA plot showed that the top-six compounds except the Hit-2 exhibit higher structural diversity compared to the native inhibitor representing strong conformational flexibility. Through the DCCM and PCA analysis, we can conclude that the binding of all other compounds except Hit-2 minimized the flexibility and escalated the correlations between the amino acid residues of the VC1 domain of the RAGE receptor.

The stability of the docked poses was demonstrated by calculating the binding free energies through the MM-GBSA approach. In our study, we preferred the compounds with dG_{bind} values of less than − 30.000 kcal/mol considering the binding affinity of the co-crystallized ligand (V6Y) (− 43.246 kcal/mol). The lead compounds, Hit-4 (− 48.487 kcal/mol) and Hit-5 (− 47.941) exhibited lower binding energies than the native ligand depicting that these compounds are more stable than others towards the RAGE receptor. Similarly, the Hit-6 compound exhibited an outstanding $\Delta G_{Coulomb}$ value of − 268.458 kcal/mol than the native ligand i.e., − 197.004 kcal/mol signifying its stability and binding into the active site of the RAGE receptor.

The per-residue decomposition analysis yielded the contributions of the consistently interacting amino acids in the binding process. It is observed that GLY_20, ALA_21, LYS_39, GLU_50, LYS_52, ARG_98, GLN_100,

LYS_110, ASN_112, and ARG_198 residues played a significant role in the binding process and contributed the most to the binding energy. The major contribution came from the residues LYS_52, ARG_98, and LYS_110 in the binding affinity for all the systems.

This study's findings could offer researchers significant insights for the development of potential RAGE inhibitors. While our study provides important insights into the identification of potential RAGE inhibitors, it is essential to acknowledge specific limitations that could have impacted the interpretation of our results and their wider acceptance. Consequently, it is essential to conduct in-vitro analysis to experimentally validate the chosen compound.

Conclusion

Alzheimer's disease is a neurodegenerative disorder of the brain, recognised as one of the most prevalent forms of dementia, constituting 60–70% of dementia cases. This underscores the potential for identifying small-molecule inhibitors through computational methods, which can tackle the challenges associated with anti-Alzheimer's disease drugs. RAGE is a cell surface receptor belonging to the immunoglobulin superfamily, capable of binding various intracellular and extracellular ligands. In humans, it exists in minimal concentrations across various healthy cell types, including the liver, kidney, lungs, brain, cardiovascular system, and immune system. Under inflammatory conditions, its expression is upregulated, contributing to the development of various diseases, including diabetes, chronic inflammation, neurodegenerative disorders, cancer, and cardiovascular diseases. This study aimed to identify potential inhibitors of the RAGE receptor (PDB Id: 6XQ3) utilizing structure-based virtual screening, molecular docking, molecular dynamics simulation, and MM-GBSA free energy calculations. According to the docking scores (XP docking scores below −6.0 kcal/mol), the resulting hit molecules were subsequently selected for molecular dynamics simulations and MM-GBSA free energy assessments. The docked compounds exhibited the expected interactions with RAGE residues, including MET_22, LYS_39, GLU_50, LYS_52, ARG_98, CYS_99, GLN_100, GLU_108, LYS_110, and ASN_112. MD simulations were conducted for the top six hits to evaluate the stability of the complexes. The MD simulation results demonstrated stable interactions between the hit compounds and the RAGE receptor throughout the 100 ns simulation, characterized by favourable protein-ligand RMSD, protein-ligand RMSF, and protein-ligand contacts. Additionally, DCCM and PCA analyses indicated significant correlations in motion among protein residues beyond those located in the active site. Compounds with dG bind scores below −30.00 kcal/mol were selected for ADME evaluation. The toxicity and drug-likeness parameters were calculated to evaluate the safety and efficacy of the selected compounds for in -vitro and preclinical experiments. Upon evaluating the results, it can be concluded that the hit-6 compound may serve as a potential inhibitor of RAGE for the treatment of Alzheimer's disease, and this research could contribute to the development of effective RAGE inhibitors in the future.

Data availability

The datasets used in the manuscript are publicly available from the repositories below: (1) Repository Name: RCSB Protein Data Bank; Deposited Date: 2020-07-09; Released Date: 2021-07-14; by source author(s): Salay, L.E., Kozlyuk, N., Gilston, B.A., Gogliotti, R.D., Christov, P.P., Kim, K., Ovee, M., Waterson, A.G., Chazin, W.J. Accession Number: https://doi.org/10.2210/pdb6XQ3/pdb; Macromolecular structure:6XQ3 [link to the reposi tory: https://www.rcsb.org/structure/6XQ3] and originally deposited from article, https://doi.org/10.1002/prot.26162, and (2) Repository Name: PubChem database [link to the repository: https://pubchem.ncbi.nlm.nih.gov/compound/155937458], and (3) other datasets generated during the current study can be made available from the corresponding author upon reasonable request.

Received: 16 December 2024; Accepted: 5 May 2025
Published online: 22 May 2025

References

1. Cummings, J. et al. Alzheimer's disease drug development pipeline: 2024. *A&D Transl Res Clin Interv* 10, e12465 (2024).
2. Cai, Z. et al. Role of RAGE in Alzheimer's disease. *Cell. Mol. Neurobiol.* **36**, 483–495 (2016).
3. Sims, J. R. et al. Donanemab in early symptomatic alzheimer disease: the TRAILBLAZER-ALZ 2 randomized clinical trial. *JAMA* **330**, 512–527 (2023).
4. van Dyck, C. H. et al. Lecanemab in early Alzheimer's disease. *N Engl. J. Med.* **388**, 9–21 (2023).
5. Sevigny, J. et al. The antibody aducanumab reduces Aβ plaques in Alzheimer's disease. *Nature* **537**, 50–56 (2016).
6. Vaz, M. & Silvestre, S. Alzheimer's disease: recent treatment strategies. *Eur. J. Pharmacol.* **887**, 173554 (2020).
7. Shukla, R., Munjal, N. S. & Singh, T. R. Identification of novel small molecules against GSK3β for Alzheimer's disease using chemoinformatics approach. *J. Mol. Graph Model.* **91**, 91–104 (2019).
8. Neeper, M. et al. Cloning and expression of a cell surface receptor for advanced glycosylation end products of proteins. *J. Biol. Chem.* **267**, 14998–15004 (1992).
9. Kong, Y. et al. Progress of RAGE molecular imaging in Alzheimer's disease. *Front. Aging Neurosci.* **12**, 227 (2020).
10. Singh, H. & Agrawal, D. K. Discovery of potential RAGE inhibitors using receptor-based pharmacophore modeling, high throughput virtual screening and Docking studies. *J. Biotechnol. Biomed.* **6**, 501–513 (2023).
11. http://www.uniprot.org/uniprot/Q15109.
12. Singh, H. & Agrawal, D. K. Therapeutic potential of targeting the receptor for advanced glycation end products (RAGE) by small molecule inhibitors. *Drug Dev. Res.* **83**, 1257–1269 (2022).
13. Sabbagh, M. N. et al. PF-04494700, an oral inhibitor of receptor for advanced glycation end products (RAGE), in Alzheimer disease. *Alzheimer Dis. Assoc. Disord.* **25**, 206–212 (2011).
14. Burstein, A. H. et al. Effect of TTP488 in patients with mild to moderate Alzheimer's disease. *BMC Neurol.* **14**, 12 (2014).
15. Shen, C. et al. RAGE-specific inhibitor FPS-ZM1 attenuates AGEs-induced neuroinflammation and oxidative stress in rat primary microglia. *Neurochem Res.* **42**, 2902–2911 (2017).
16. Liu, Y. et al. Inhibition of RAGE by FPS-ZM1 alleviates renal injury in spontaneously hypertensive rats. *Eur. J. Pharmacol.* **882**, 173228 (2020).

17. Paudel, Y. N. et al. Impact of HMGB1, RAGE, and TLR4 in Alzheimer's disease (AD): from risk factors to therapeutic targeting. *Cells* **9**, 383 (2020).
18. Kozlyuk, N. et al. A fragment-based approach to discovery of receptor for advanced glycation end products inhibitors. *Proteins* **89**, 1399–1412 (2021).
19. Berman, H. M. The protein data bank. *Nucleic Acids Res.* **28**, 235–242 (2000).
20. *Schrödinger Release 2024-1: Protein Preparation Wizard* (Epik, Schrödinger, LLC, 2024).
21. *Schrödinger Release 2024-1: Glide* (Schrödinger, LLC, 2024).
22. *Schrödinger Release 2024-1: LigPrep* (Schrödinger, LLC, 2024).
23. *Schrödinger Release 2024-1: Prime* (Schrödinger, LLC, 2024).
24. Gupta, A., Chaudhary, N. & Aparoy, P. MM-PBSA and per-residue decomposition energy studies on 7-phenyl-imidazoquinolin-4(5H)-one derivatives: identification of crucial site points at microsomal prostaglandin E synthase-1 (mPGES-1) active site. *Int. J. Biol. Macromol.* **119**, 352–359 (2018).
25. Dash, S., Rathi, E., Kumar, A., Chawla, K. & Kini, S. G. Identification of DprE1 inhibitors for tuberculosis through integrated in-silico approaches. *Sci. Rep.* **14**, 11315 (2024).
26. Shah, S. K. et al. Multi-target in-silico modeling strategies to discover novel angiotensin converting enzyme and Neprilysin dual inhibitors. *Sci. Rep.* **14**, 15991 (2024).
27. *Schrödinger Release 2024-1: Phase* (Schrödinger, LLC, 2024).
28. *Schrödinger Release 2024-1: Desmond Molecular Dynamics System* (D. E. Shaw Research, 2024).
29. Pirolli, D. et al. Virtual screening and molecular dynamics simulations provide insight into repurposing drugs against SARS-CoV-2 variants Spike protein/ACE2 interface. *Sci. Rep.* **13**, 1494 (2023).
30. Thapa, B. & Raghavachari, K. Energy decomposition analysis of protein–ligand interactions using molecules-in-molecules fragmentation-based method. *J. Chem. Inf. Model.* **59**, 3474–3484 (2019).
31. Xiong, G. et al. ADMETlab 2.0: an integrated online platform for accurate and comprehensive predictions of ADMET properties. *Nucleic Acids Res.* **49**, W5–W14 (2021).
32. Chauhan, A. et al. An insight into the simulation directed Understanding of the mechanism in SARS CoV-2 N-CTD, dimer integrity, and RNA-binding: identifying potential antiviral inhibitors. *J. Biomol. Struct. Dyn.* **40**, 13912–13924 (2022).
33. Dash, R. et al. Unveiling the structural insights into the selective Inhibition of protein kinase D1. *Curr. Pharm. Des.* **25**, 1059–1074 (2019).
34. Bhakat, S., Martin, A. J. M. & Soliman, M. E. S. An integrated molecular dynamics, principal component analysis and residue interaction network approach reveals the impact of M184V mutation on HIV reverse transcriptase resistance to lamivudine. *Mol. Biosyst.* **10**, 2215–2228 (2014).
35. Serrano-Pozo, A., Frosch, M. P., Masliah, E. & Hyman, B. T. Neuropathological alterations in alzheimer disease. *Cold Spring Harb Perspect. Med.* **1**, a006189 (2011).
36. Heneka, M. T. et al. Neuroinflammation in Alzheimer's disease. *Lancet Neurol.* **14**, 388–405 (2015).
37. Suresh, J. et al. Shared signaling pathways in Alzheimer's and metabolic disease May point to new treatment approaches. *FEBS J.* **288**, 3855–3873 (2021).
38. Waugh, M. L. et al. Modulating the RAGE-induced inflammatory response: peptoids as RAGE antagonists. *Chembiochem* **24**, e202300503 (2023).
39. Hofmann, M. A. et al. RAGE mediates a novel Proinflammatory axis: a central cell surface receptor for S100/calgranulin polypeptides. *Cell* **97**, 889–901 (1999).
40. Hori, O. et al. The receptor for advanced glycation end products (RAGE) is a cellular binding site for amphoterin. Mediation of neurite outgrowth and co-expression of Rage and amphoterin in the developing nervous system. *J. Biol. Chem.* **270**, 25752–25761 (1995).
41. Santilli, F., Vazzana, N., Bucciarelli, L. G. & Davì, G. Soluble forms of RAGE in human diseases: clinical and therapeutical implications. *Curr. Med. Chem.* **16**, 940–952 (2009).
42. Xie, J., Méndez, J. D. & Méndez-Valenzuela, V. Aguilar-Hernández, M. M. Cellular signalling of the receptor for advanced glycation end products (RAGE). *Cell. Signal.* **25**, 2185–2197 (2013).
43. Batkulwar, K. B. et al. Investigation of phosphoproteome in RAGE signaling. *Proteomics* **15**, 245–259 (2015).
44. Burstein, A. H. et al. Development of Azeliragon, an oral small molecule antagonist of the receptor for advanced glycation endproducts, for the potential slowing of loss of cognition in mild Alzheimer's disease. *J. Prev. Alzheimers Dis.* **5**, 149–154 (2018).
45. Hong, Y. et al. Effects of RAGE-specific inhibitor FPS-ZM1 on amyloid-β metabolism and AGEs-induced inflammation and oxidative stress in rat hippocampus. *Neurochem Res.* **41**, 1192–1199 (2016).
46. Cary, B. P. et al. Synthesis and evaluation of [(18)F]RAGER: A first generation small-molecule PET radioligand targeting the receptor for advanced glycation endproducts. *ACS Chem. Neurosci.* **7**, 391–398 (2016).

Author contributions

S.R. and I.B. contributed to the study's conception and design. I.B. and V.P. performed all the computational work and data analysis. I.B. wrote the main manuscript and also prepared all the figures and tables in the text. S.R. critically reviewed and edited the manuscript. All authors read and approved the final version of the manuscript.

Declarations

Competing interests

The authors declare no competing interests.

Additional information

Supplementary Information The online version contains supplementary material available at https://doi.org/10.1038/s41598-025-01271-0.

Correspondence and requests for materials should be addressed to S.R.

Reprints and permissions information is available at www.nature.com/reprints.

Publisher's note Springer Nature remains neutral with regard to jurisdictional claims in published maps and institutional affiliations.